9-1-2018

The synthesis and characterization of a magnetite nanoparticle with potent antibacterial activity and low mammalian toxicity

Seyedeh Maryamdokht Taimoory
University of Windsor

Abbas Rahdar
University of Zabol

Mousa Aliahmad
University of Sistan and Baluchestan

Fardin Sadeghfar
University of Sistan and Baluchestan

Mohammad Reza Hajinezhad
University of Zabol

See next page for additional authors

Authors

Seyedeh Maryamdokht Taimoory, Abbas Rahdar, Mousa Aliahmad, Fardin Sadeghfar, Mohammad Reza Hajinezhad, Mohammad Jahantigh, Parisa Shahbazi, and John F. Trant

The Synthesis and Characterization of a Magnetite Nanoparticle with Potent Antibacterial Activity and Low Mammalian Toxicity

Seyedeh Maryamdokht Taimoory[a], Abbas Rahdar[b,*], Mousa Aliahmad[c], Fardin Sadeghfar[c], Mohammad Reza Hajinezhad [e], Mohammad Jahantigh[f], Parisa Shahbazi[f], John F. Trant[a,*]

[a] *Department of Chemistry and Biochemistry, University of Windsor, Windsor, ON N9B 3P4, Canada;* [b] *Department of Physics, University of Zabol, Zabol, Iran;* [c]*Department of Physics, University of Sistan & Baluchestan, Zahedan, Iran;* [e]*Assistant Professor of physiology, Basic Science Department, Faculty of Veterinary Medicine, University of Zabol, Zabol, Iran;* [f] *Department of Clinical Sciences, School of Veterinary Medicine, University of Zabol, Zabol, Iran*

*****Prof. John F. Trant: Department of Chemistry and Biochemistry, University of Windsor, 401 Sunset Avenue, Windsor, ON, N9B 3P4, Canada; **phone:** 1-519-253-3000 xt3528; **fax**: 1-519-973-7098 j.trant@uwindsor.ca; *****Prof. Abbas Rahdar: Department of Physics, University of Zabol, Zabol, P. O. Box. 35856-98613, Islamic Republic of Iran; **phone:** +98-91-53434909; **fax**: +98-54-22230540; a.rahdar@uoz.ac.ir; Prof. Mousa Aliahmad: Department of Physics, University of Sistan and Baluchistan, Zahedan, Iran , P. O. Box. 98155-987, Islamic Republic of Iran; **phone**: +98-91-51903677; **fax:** +98-54-33446251; aliahmad@phys.usb.ac.ir.

The Synthesis and Characterization of a Nanomagnetite with Potent Antibacterial Activity and Low Mammalian Toxicity

Graphical Abstract

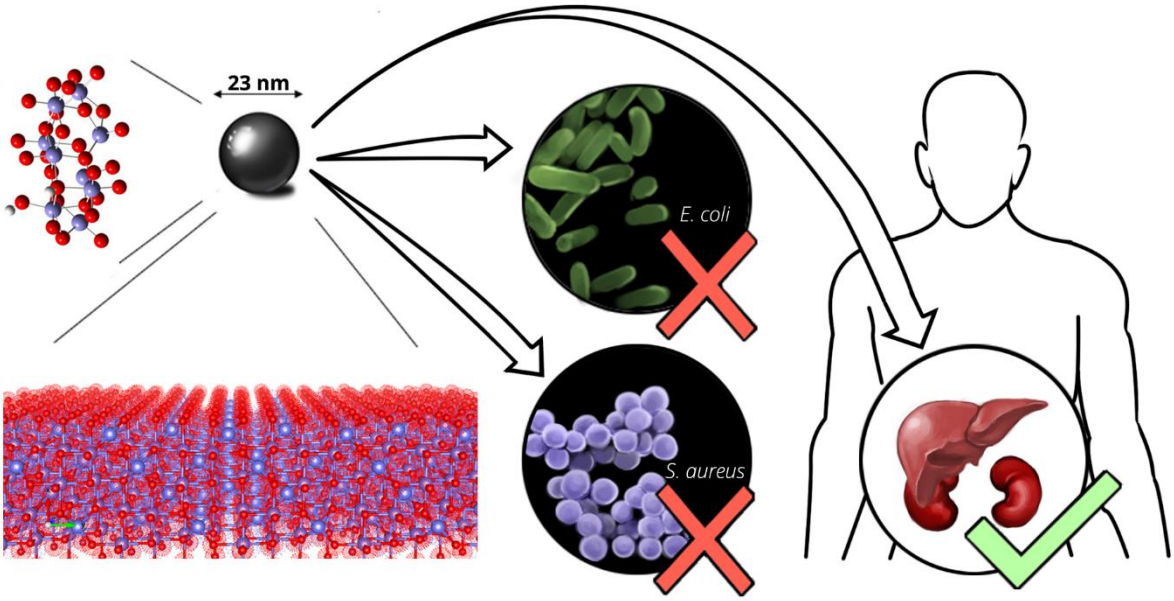

Abstract

Magnetite has shown some promise as a biomedical material and antibacterial agent; however the benefits are normally only realized when it is used in combination with other metals or drugs. Unfunctionalized magnetite may be a biocompatible alternative. This report discusses the synthesis and potent antibacterial activity, with low associated mammalian organ toxicity, of nanomagnetite particles. Magnetite (Fe_3O_4) nanoparticles were electrochemically prepared in a green surfactant-free, closed water loop system. These materials, characterized by X-ray diffraction, FTIR, and vibrational magnetometry, also appear contaminated with Fe-O-O-H functionalities. This physical characterization is accompanied by a computational investigation of truncated clusters showing that a magnetite-derived cluster of 7 iron atoms is a sufficient model to generate the vibrational frequencies experimentally observed in magnetite using DFT calculations. The nanoparticles, evaluated for antibiotic activity, were shown to have minimum inhibitory concentrations of 2.8 and 2.0 µg/mL against *E. coli* and *S. aureus* respectively. This is both a 100-fold lower concentration than the human cytotoxic dose determined by an MTT assay and is

also comparable to the effective dose of traditional antibiotics. A dose-dependent decrease in catalase activity and an increase in the levels of lipid peroxidation suggests that these nanoparticles act through damaging the anti-oxidant systems in cells. However, renal and hepatic damage was only observed at daily doses (2 weeks) of 100 μg/mL and higher. This significant therapeutic window suggests that these materials might prove useful as potential complementary therapeutics in the future.

Keywords: nanomagnetite; antibiotic; density functional theory; electrochemical synthesis.

1. Introduction:

In recent years magnetite (Fe_3O_4) nanomaterials have drawn significant biomedical interest. The ability to control size and dispersity through careful tuning of the synthetic parameters, along with their unique superparamagnetic properties and low toxicity make them highly promising materials for applications in hyperthermic therapy, targeted drug-delivery, contrast agents for magnetic resonance imaging, cell separation, and immunoassays.[1-10] There are many ways to prepare nanomagnetite particles including using sol-gels,[11] hydrothermal approaches,[12] solid state milling,[13] wet milling,[14] pyrolysis,[15] and microemulsion formation.[16] However, electrochemistry is a particularly promising production method, as it requires no complex sample preparation.[17, 18] Furthermore, this approach allows for simple control of the particle size, and hence its properties, by adjusting the current density, the distance between the electrodes and/or the voltage potential. A preferred iteration of this strategy is to dispense with the surfactants that are often employed to provide a more uniform dispersity of materials and prevent micro-aggregation. These surfactants, often difficult to fully remove following synthesis, are, due to their very nature, toxic to biological systems at moderate concentrations and can also physically encapsulate other

impurities. The surfactant-free synthesis of nanoparticles has been reported,[19, 20] but to the best of our knowledge, no studies have examined the effect of the reaction pH on the resulting materials. We have previously shown that the syntheses of nanomagnetite nanoparticles can be accomplished using a closed-water loop, without the need for inert carrier gases.[21] In that study we reported our efforts in tuning the properties of the nanoparticles by simply changing the distance between the electrodes. We then examined the cytotoxicity of our nanoparticles using a standard colourometric toxicity assay employing 3-(4,5-dimethylthiazol-2-yl)-2,5-diphenyltetrazolium bromide, the MTT assay, and demonstrated that they show no appreciable toxicity at doses as high as 200 μg/mL. However, the mechanism of cytotoxicity was not investigated. The experimental and theoretical XRD analysis of those particles also suggested the presence of Fe-O-O-H functional groups, and this raises the possibility that these materials act through initiating an oxidative damage cascade. These functionalities are not accessible on the surface of core-shell iron oxide nanoparticles. In these standard formulations, the iron oxide core is coated with a silica, other metal, organic, or other coating insulating the core from interaction with the environment.[22, 23] The presence of these reactive functionalities on the surface of our proposed systems might provide the nanoparticles with interesting biological activity. This result required further investigation, especially as they might prove to be potential non-classical antibiotics.

Antibiotic resistance is a growing challenge to public health world-wide.[24] As improper use and over-reliance on these medications has increased, a growing number of highly resistant “super-bugs” have been identified. The search for new chemical antibiotics has slowed over recent decades, and having a non-traditional option might prove to be very useful in the future.[25] Iron oxide nanoparticles have been proposed to be excellent potential candidates, and have been investigated for this application, but

always in combination with other materials.[26, 27] They have almost always been used as coated nanoparticles,[28] and on their own have not been found to inhibit culture growth except at quite high concentrations,[29] or have required the presence of another metal like silver.[26, 30] Our current materials are not capped with an organic surfactant. Due to the presence of the oxidative impurities that result from our synthesis and their small size,[31] they appear to be reasonably stable to aggregation; no microscopic particle formation or turbidity is observed upon standing for several weeks. *E. coli* (gram negative) and *S. aureus* (gram positive) are two of the best studied microbes and are excellent model organisms for more dangerous bacterial pathogens,[32] and consequently make excellent model organisms.

Consequently, we wish to report our studies into the effect of pH on nanomagnetite synthesis anda more detailed computational model of magnetite. In addition, we wish to discuss our investigations into the antibacterial potential of these materials, and our preliminary studies into their mechanism of toxicity and their effect on renal and hepatic health.

2. Material and Methods:

2.1 General experimental information:

Iron (II) sulfate heptahydrate ($FeSO_4 \cdot 7H_2O$, Sigma-Aldrich) and sodium hydroxide (Sigma-Aldrich) were analytical grade and used as received without further purification. The DU145 human adenocarcinoma cell line was purchased from the Pasteur Institute (Iran). X-ray powder diffraction was carried out on a D8 Advance X'Pert X-Ray diffractometer (Bruker). Fourier-transform infrared spectroscopy was done on a JASCO 640 plus machine (4000-400 cm^{-1}) at room temperature using KBr pellets. Vibrating magnetometry was analyzed using a Kavir Precise Magnetic instrument (MDKFT,

Iran). Field emission scanning electron microscopy was carried out using a Mira 3-XMU instrument capable of 700,000x magnification.

2.2 Nanoparticle synthesis:

The magnetite nanoparticles were synthesized using our previously published green surfactant-free electrochemical method.[21] This protocol requires no inert gas and is accomplished in a closed water loop system at ambient temperatures and pressures. A solution of iron (II) sulfate, under basic conditions, is induced to form nanoparticles on the surface of steel plates placed within a constant electric field. In the present study, the precise nature of the particles was tuned by changing the pH of the reaction solution using NaOH. Particles were prepared at three different pHs, 10.00, 12.30, and 13.00. All three conditions provided black precipitates that were then analyzed to determine the effect that alkalinity has on particle size and nature. We have previously published the data from the pH=13.00 sample in a study on the effect of electrode spacing on the properties of the nanoparticles.[21] The data is included here for comparison purposes, and to highlight the importance of pH on these same properties.

Additional details are provided in the SI.

2.3 Computational methodology:

The computational calculations for our proposed iron oxide clusters (**Fe_4**, **Fe_5**, **Fe_7**, and **Fe_9**) were performed using the Gaussian 09 suite of programs.[33] Additional details are provided in the SI.

2.4 Ethics review:

The following biological research was all approved by the ethics board at the University of Zabol (Ref:2-8-93). The animal studies were conducted following the guidelines of the Animal Ethics Committee of the Faculty of Veterinary Medicine, University of Zabol, Zabol, Iran (Ref:2-8-93). All animal treatment was carried out in a humane fashion in compliance with both institutional and EU Directive 2010/63/EU requirements.

2.5 Antibacterial assay:

The determination of the minimum inhibitory concentration (MIC) was carried out in 96-well plates using serial dilutions of a stock of sonicated 3000MP Ultrasonic Homogenizer) nanoparticles (those prepared as above at pH =13) according to the standard protocol.[34] *Escherichia coli* and *Staphylococcus aureus* were prepared from human diagnostic laboratories and identified using standard bacteriological methods.[35] Additional details are provided in the SI.

2.6 Animal studies:

All weights are dry weights. Adult male Wistar rats (190- 210 g) obtained from the Laboratory Animal Center University of Zabol were used in this study. Rats were randomly divided into four groups (n =10). The control group was given 1 ml of distilled water using the oral gavage technique once a day for 14 days. The second group was treated with 1 mL of nanomagnetite solution (10 ppm/ml/day) once a day, for 14 days. The third group received 1 mL of nanomagnetite solution (100 ppm/ml/day) once a day, for 14 days. The fourth group received 1 mL of nanomagnetite solution (1000 ppm/ml/day) once a day, for 14 days. At the end of the feeding schedule (14 days) the animals were sacrificed by cervical dislocation and the blood samples

were collected from the heart and centrifuged (3000 rpm for 5 min) to recover the serum. The serum was then immediately frozen at −80 ºC until needed for the assays detailed in the supporting material and described below.

3. Results and Discussion:

3.1 Description of Fe_3O_4 molecular structure:

In the spinel form (Figure 1), the oxygen ions of Fe_3O_4 have a close packed orientation along the [1 1 1] direction and this separates adjacent Fe ion layers into two different arrangements (Figure 1b). In the first arrangement Fe ions are present in both octahedral (Fe_{oct}) and tetrahedral (Fe_{tet}) geometries; in the other layer, all of the Fe ions adopt the Fe_{oct} orientation.[36] As shown in Figure 1c, each unit cell is composed of four rhombohedral primitive cells. This is a far more complicated structure than that of other forms of iron oxide such as Fe_2O_3, and FeO; Fe_3O_4 has iron ions in mixed valence and is better described by the formula $Fe_{tet}^{3+}Fe_{oct}^{2+}Fe_{oct}^{3+}O_4$.

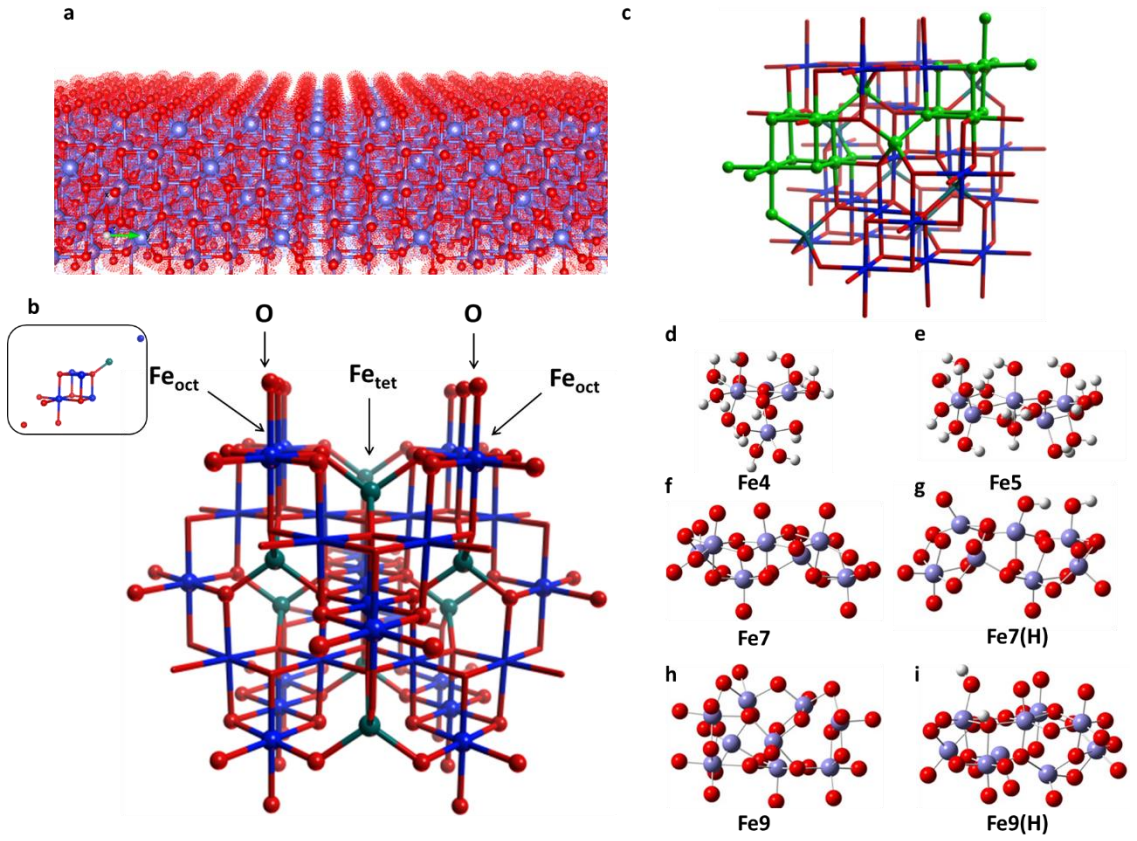

Figure 1. In all images, iron is represented as blue, and oxygen as red. **a)** Visualization of the magnetite supercell represented by a ball and stick model together with dot surfaces representing the outer surfaces of atoms; **b)** Ball and stick model of the cubic unit cell showing the tetrahedral Fe atoms in turquoise, and the octahedral Fe atoms in blue. Layer A is indicated using balls for the atoms; layer B represents the atoms as the points of intersection of the tubes; **c)** A top down view of the same cluster as in b). Two primitive unit cells are outlined in bright green. Quantum chemically calculated lowest energy structures and the optimized geometry for our selected clusters: **Fe4 (d)**, **Fe5 (e)**, **Fe7 (f)**, **Fe7(H)**; which is the same core structure as **Fe7**, but with two additional hydrogens (on the top right), imitating the surface of nanomagnetite rather than a sample from the core of a particle **(g)**, **Fe9 (h)**, and a diprotonated **Fe9(H) (i)**. a) was prepared with VESTA, b and c were prepared using MOE, and d-i are Gaussview visualizations of the optimized structures. **Fe4** and **Fe5** were optimized using DFT theory, while **Fe7** and **Fe9** were optimized using a semi-empirical PM6 method.

In our recent report, we disclosed the density functional theory derived structures of four (**Fe4**) and five (**Fe5**) iron-atom magnetite clusters.[21] Earlier reports have discussed the geometry and electronic structure of simple magnetite model clusters

containing 1-3 iron atoms.[37-40] However, as magnetite contains three distinct iron atoms in non-equal amounts, these earlier magnetite models are possibly insufficient for properly defining the nature of the material. Although we extrapolated certain physical parameters from these calculations, the complexity of magnetite might not have been sufficiently accurately modelled using our singlet **Fe5** system. This became important especially when we saw a significant improvement in the quality of the predicted vibrational spectrum for the **Fe5** vs the **Fe4** system. We wish to report the results from our optimized structures at different spin multiplicities, and the extension of our work to higher order complexes with 7 (**Fe7**) or 9 (**Fe9**) iron atoms, both with and without surface hydrogen atoms (Figure 1c-h).

Our previously reported **Fe4** and **Fe5** clusters were initially reoptimized at higher-spin states (M = 15, 17, and 19) using unrestricted B3LYP exchange-correlation functionals at the 6-31G** and/or 6-311++G** level of theory (Table 1).

Table 1. Calculated relative energies (selective results), Fe-Fe bond lengths, total spin representing the amount of spin contaminations, and full magnetic spin momentum of the various magnetite clusters discussed in this report.

	Multiplicity *M*	**Total spin $\langle S^2 \rangle$**	**ΔE(B3LYP) and/or ΔE(PM6) relative to lowest E system (kcal/mol)**	**Fe-Fe bond length (Å)**	**Full magnetic spin momentum ($2[S(S+1)]^{1/2}$) (μB)**
Fe4	1	0.0	69.0	2.92	N/A
	15	56.2	2.8	2.97	14.97
	17	72.3	0.0	3.04	16.97
Fe5	1	0.0	59.0	2.94	N/A
	19	90.1	0.0	2.93	18.97
Fe7	1	0.0	28.1	2.79	N/A
	5	9.69	0.0	2.80	4.90
	7	14.71	2.1	2.76	6.93
Fe9	1	0.0	11.8	2.79	N/A
	5	9.17	0.0	2.80	4.90
	7	14.25	1.8	2.79	6.93

The lowest **Fe4** energy structure corresponded to a high-spin state of the cluster, (multiplicity, M = 17), while the lowest energy for **Fe5** was obtained with M = 19, both with negligible spin contaminations. The calculated interatomic Fe–Fe bonds lengths for these optimized structures, were 3.04 Å and 2.93 Å, respectively. The interatomic Fe–Fe distances in the **Fe5** cluster at both low (M = 1) spin and high spin states (M = 19) are a good match with the shortest Fe–Fe bond length in the bulk magnetite (2.96 Å). This protonated **Fe5** cluster consequently continues to represent a good model of the nanomagnetite surface.

For the larger systems, **Fe7** and **Fe9**, due to the complexity of the system, the DFT self-consistency procedure did not converge. Consequently, we resorted to optimizing these clusters using the semiempirical quantum-chemical method, PM6, with both restricted wavefunctions (RHF) and unrestricted wavefunctions (UHF).. Although these semiempirical methods are not considered as accurate as DFT, for these highly organized systems the difference is generally minimal: recently, for a three-iron minimal magnetite cluster it was found that both PM6 and DFT yielded similar results.[40] Our comparison of the DFT and PM6 (data not shown) simulations of the **Fe4** and **Fe5** systems supports this result. The total energies, ΔE_{tot}, of the **Fe7** and **Fe9** clusters at different spin multiplicities (M) of the electronic state were calculated. For both **Fe7** and **Fe9**, three energy minima were found by the PM6 method and in both cases the lowest energy state was found at M=5. The next lowest energy **Fe7** and **Fe9** structures corresponded to the spin-state of M = 7 structures and lie 2.1 and 1.8 kcal/mol higher in energy respectively. For paramagnetic systems, the accuracy of the calculations also depends on the degree of spin contamination. As with the energy, the spin contamination was lower at M = 5 state than in the M =7 system. Thus, both the energy calculation and spin contamination

parameters converged on the same solution. These M = 5 **Fe7** and **Fe9** clusters form promising preliminary models for expansion into larger magnetite model clusters of Fe_3O_4.

The surface of our nanomagnetite is functionalized with hydroxyl groups. To reflect this feature of the nanoparticle surface, we also optimized cluster models, **Fe7(H)** and **Fe9(H)**, in which the valences of some of the terminal Fe-O functionalities were capped with hydrogens (Figure S1). It does not appear that the system is greatly distorted by the presence or absence of these protons. The Fe-Fe bond length is, however, calculated to be a bit shorter in these hydrogenated clusters. These appear to be good minimum clusters for acting as the theoretical model for Fe_3O_4, magnetite, and could prove useful for further advanced DFT-based and ab initio analysis of these systems in the future. With these calculations in hand, we compared our results to the experimental characterization.

3.2 Magnetic and Physical Characterization:

The materials were first examined by powder XRD (Figure 2a). The Bragg peaks at 2θ values of 30.5° (2 2 0), 35.9° (3 1 1), 37° (2 2 2), 43.5° (4 0 0), 57.3° (5 1 1), 63.1° (4 4 0) and 74.1° (5 3 3) are the expected signals from Fe_3O_4.[41] However, like in our previous study, peaks due to FeOOH can also be observed.[42] This contamination appears to be an inevitable byproduct of our electrochemical synthetic process, and may be responsible for some of their biological activity. As in our previous report, the experimental XRD plot is compared with the theoretical XRD derived from our computational model, shown in Figure 2b along with the calculated spectra of two other iron oxides, Fe_2O_3, and FeO (Figure 2c-d). This highlights the complex nature of the spectrum derived from the mixed valence Fe_3O_4 compared with other iron oxides, and

also strongly suggests that neither of these other two materials is present in our nanoparticles as significant contaminants.

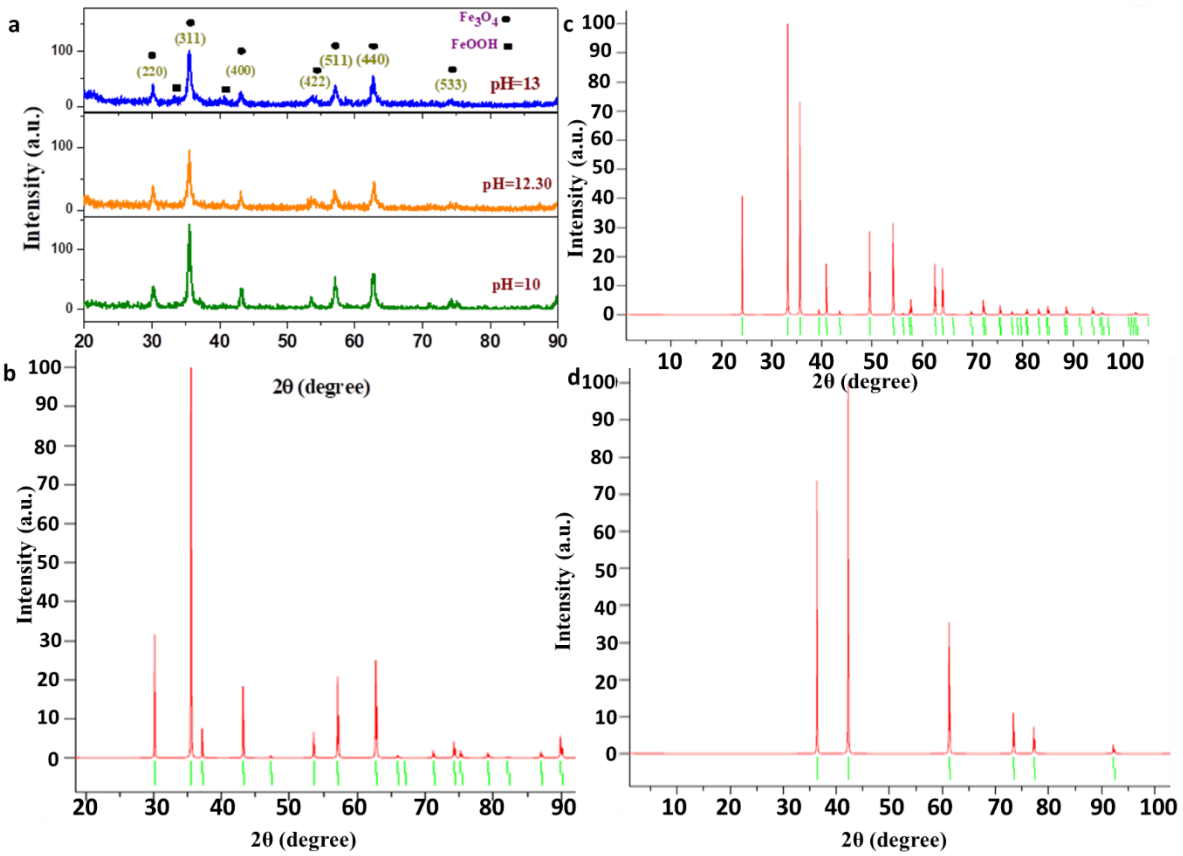

Figure 2. Experimental and calculated Powder XRD spectra of the iron magnetite nanoparticles. **a)** XRD spectra of the nanomagnetite prepared in this study at the different pHs, Bragg peaks due to magnetite (●) and peroxide-functionalized iron (■) are labelled; **b)** Calculated XRD of nanomagnetite, spectrum has been truncated at low and high angles to match the experimental results for easy comparison; **c)** Calculated XRD of nanohematite (Fe_2O_3); **d)** Calculated XRD of nanowüstite (FeO). All plotted spectra were derived from calculations made with VESTA.

The average diameters of the nanocrystals were extracted using the Scherer formula ($D_{h,k,l} = \frac{0.9\lambda}{\beta_{h,k,l} \cdot cos\theta}$, where λ is the wavelength (λ= 1.542 Å, CuK_α source); β is the peak width at half height of the signal and θ is the diffraction angle) using the (3 1 1) plane reflection from the XRD pattern (Table 2).[43]

Table 2. Size of the prepared nanoparticles synthesized as a function of *pH* as determined by XRD.

Nanoparticle	***pH***	**Nanoparticle average diameter (nm)**
a	13	**19**
b	12.30	**21.4**
c	10	**23**

As the pH increases, nanoparticle diameter decreases. We have previously observed that smaller particles are representative of a slower reaction, which initiates more nucleation sites, and hence more, but smaller, particles;[21] this appears to suggest that as the pH increases, the rate of reaction is slowed. Furthermore, as we increased the concentration of $^{-}$OH, the crystallinity of the product appears to decrease.

Fourier transform IR analysis was performed to determine if the precise nanostructured formulation affects the spectrum (Figure 3).

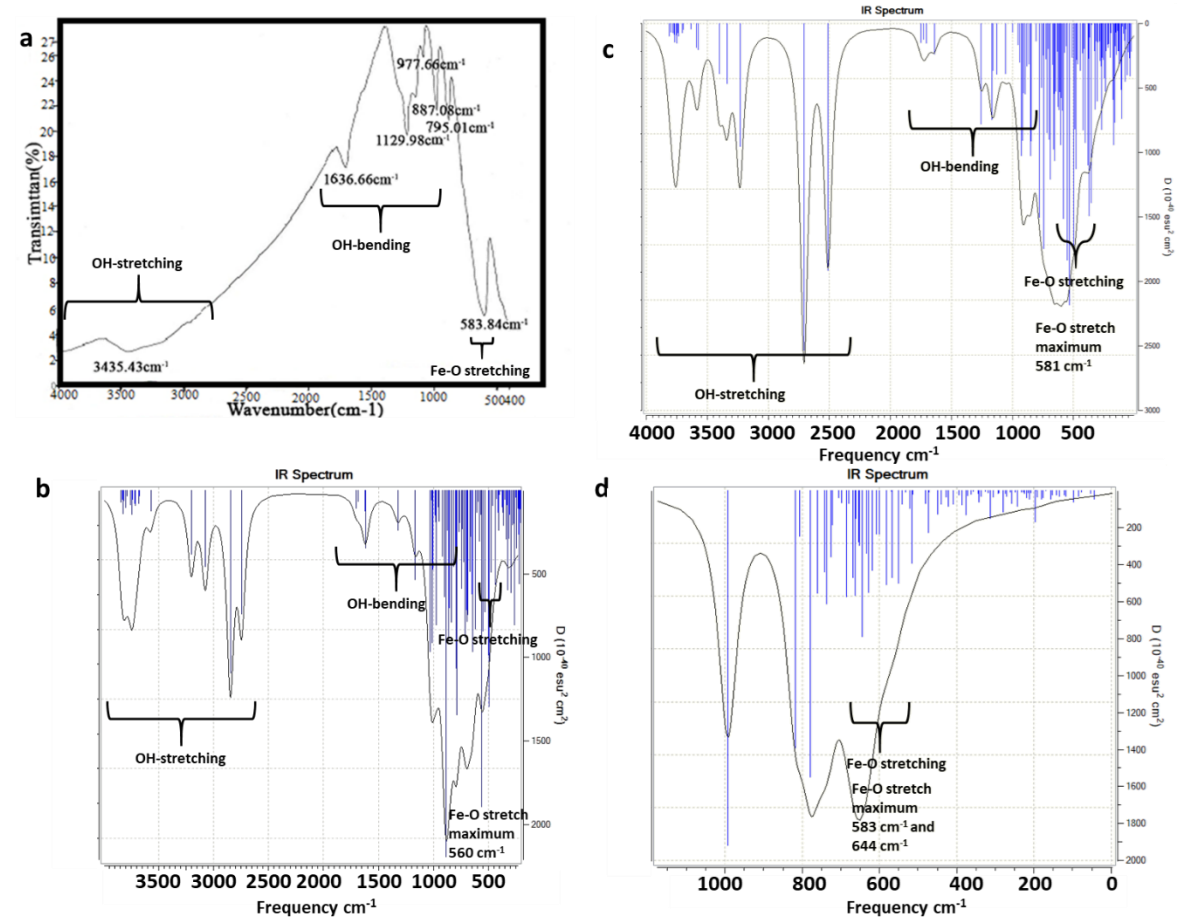

Figure 3. **a**) Transmittance FTIR spectrum of synthesized sample a (*pH* = 13.00). No baseline correction was applied, transmittance minima are labelled; **b**) Calculated FTIR spectrum of our **Fe5**, *M* = 1 simulation (reproduced with permission from reference [10]); **c**) Calculated FTIR spectrum of our **Fe5**, *M* = 17 simulation; **d**) Calculated FTIR spectrum of our **Fe7**, *M* = 5 simulation. For the simulated spectra, blue lines are the calculated vibrations, the black curve represents the linear combination of these values. Vibrational regions are labelled for convenience; note that due to the small size of the cluster in **B** and **C**, a larger proportion of hydroxyl groups are present, these very strong O-H stretches at high wavenumbers are not expected in the experimental spectrum. These peaks are completely lacking from **D** where no hydrogen atoms are included in the cluster. Simulated spectra were produced using GaussView 5.0.9 setting the IR peak Half-Width at Half Height value to 25 cm^{-1} to generate the spectra (black lines) from the calculated vibrations.

There was no significant difference between the FTIR spectra of the three samples, and the FTIR of sample **c** is provided as Figure 3a. The broad band at 3440 cm^{-1} is

consistent with an O-H stretching vibration from either O-H or O-O-H surface functionalization. The bending mode for this functionality can be observed by the peak at 1640 cm^{-1}. The other major peak observed at 583 cm^{-1} is in the typical range observed for the Fe-O stretch in magnetite derived nanoparticles.[41, 44] The strong resonance at 1130 cm^{-1} can be ascribed to C-O stretching, possibly arising from surface functionalization with carbon dioxide. The strong bands at 888 cm^{-1} can be ascribed to Fe-OH,[45] and the one at 795 cm^{-1} to Fe-O-O-H.[46] These peaks were not as sharp as those in our previous study.[21] To further describe this spectrum, and to better differentiate the usefulness of our various computational cluster models, we also generated IR spectra from the predicted frequencies arising from these structures. As the computational clusters are small, and were primarily focused on examining the magnetic profile, and aimed at providing a useful model of Fe_3O_4 in truncated form for other researchers in the field, we capped the iron with oxygens (Fe-OH or $Fe\text{-}O^-$). Thus, the calculated FTIR of these generated truncates was only a useful model for discussing the frequencies of the core Fe-O vibrations but not for the other peaks observed in the experimental spectrum. The IR spectra of magnetite generally contains a signal of medium intensity at 440 cm^{-1} arising from the octahedral Fe–O vibration, and an intense broad band at 590 cm^{-1} associated with vibrations of Fe-O tetrahedral sites.[40] Figure 3B shows our previously reported calculated IR spectrum arising from the **Fe5** at *M*=1 structure. The Fe-O maximum is at 560 cm^{-1}. However, when we correct for the *M*=17 spin system, the vibration shifts to 581 cm^{-1} (Fig 3C). The **Fe7** and **Fe9** systems behave similarly, and the **Fe7**, *M*=5 spectrum is provided as Figure 3D. This slightly larger system modifies the predicted vibration to 583 cm^{-1} which absolutely matches the experimental result; there is an additional stretch maximum at 644 cm^{-1}, which is consistent with the shoulder observed in Figure 3A. This larger

cluster appears to provide a slightly more accurate estimation of the vibrational frequencies than the smaller **Fe5** cluster. This is to be expected as the complex structure of magnetite is better approximated by the system containing more iron atoms, and consequently this model, Fe7 may prove useful as an improved minimum computational model for studying magnetite, specifically pave the path for justification of the spectroscopic behaviour of both pure and contaminated nanomagnetite.

Materials were further characterized through vibrational magnetography which showed that the magnetic saturation is considerably lower than that observed in bulk Fe_3O_4 (≈92 emu/g),[47, 48] as is expected for a nanoformulation. The smaller particle also has the smaller saturation as expected. Magnetic remanence follows the same pattern, but the size of these nanoparticles ensures that they maintain ferromagnetic properties rather than lose remanence all together. Coercivity reads either 0 or 100 for these materials, which is in complete agreement with the expected values for randomly oriented, non-interacting magnetite particles.[20]

The saturation magnetization, M_s, of the nanoparticles is dependent on the pH of the synthesis mixture (Figure 4a).

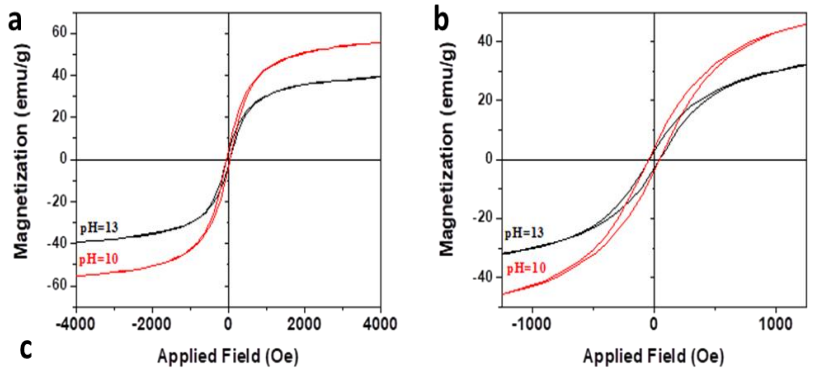

Sample	Diameter (nm)	(Magnetic Remanence) M_r (emu/g)	H_c (Coercivity) (Oe)	(Magnetic saturation) M_s (emu/g)
a	19	2.97	0	42.4
c	23	3.97	100	59.3

Figure 4. Vibrational magnetography. **a)** Magnetograph obtained of two of the samples (**a**, prepared at pH=13, and **c**, prepared at pH=10); **b)** Expansion of **a** to highlight the hysteretic loop in the sigmoidal curve; **c)** Table of the magnetic parameters.

In our previous work we showed that the 19 nm diameter particle behaved nearly identically to a 23 nm particle (both were prepared at pH=13);[21] however, this 23 nm particle shows much greater amplitude in the sigmoidal curve. This difference might be due to changes in the crystallinity of the magnetite that results from the different pHs. The presence of a hysteretic loop (Figure 4b) in the rapidly changing region is characteristic of ferromagnetic materials larger than 10 nm.[20, 49] The origin of this hysteretic effect has been variously ascribed to the pinning of magnetic domain walls to grain boundaries, to impurities within the lattice or due to the intrinsic magnetic anisotropy of the crystal lattice.[20, 43, 49] The magnetic parameters are provided in Figure 4c.

Our computational models provide the total spin magnetic moment for the computed clusters that differs from that of bulk magnetite (4 μB/formula unit). We obtained values of between 14.97 and 18.97 μB/formula unit) for our DFT analyzed **Fe4** and **Fe5** clusters (the PM6 optimized **Fe7** and **Fe9** clusters provided much smaller magnetrons comparable to bulk magnetite as they are not capped with hydrogen functionalities, of 4.9 μB/formula unit). The **Fe4/5** values are consistent with that which has been observed for ferromagnetite thin films where magnetic moments of 13.6 and 17.4 μB per formula unit have been observed.[50] The magnetic properties of our optimized iron oxide clusters were calculated from the full magnetic spin moment S,2[S(S + 1)]$^{1/2}$ in Bohr magnetons μB.

FESEM imaging was also carried out on the sample (Figure 5).[21] The XRD analysis estimated a diameter of 19 nm, which is consistent with the apparent size of the

nanoparticle features in these images. The deposition of distinct nanoparticles is consistent with the observed lack of solution nanoaggregation, as we would expect to see a degree of Oswald ripening in that case

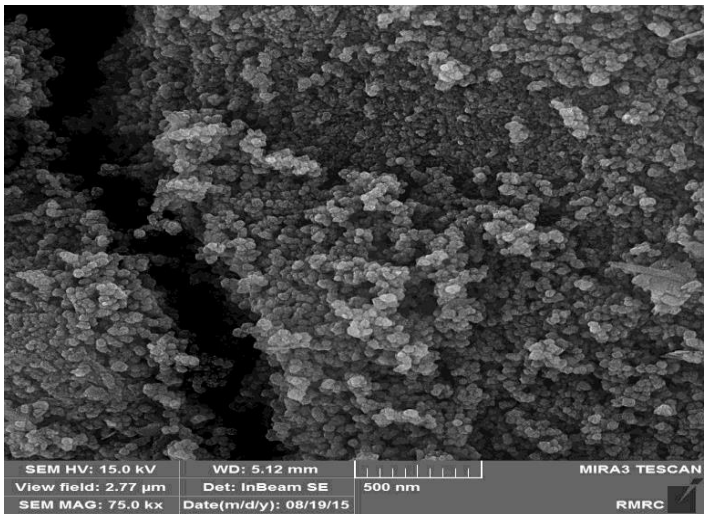

Figure 5. FESEM image of the nanoparticles deposited on a silicon wafer. Note the relative uniformity of the nanoparticles on the surface.

Consequently, by modifying the pH, we are able to generate materials with diameters between 19 and 23 nm. In our previous study, by modifying the distance between electrodes, we were able to generate materials with diameters between 19 (6 cm) and 33 (2 cm) nm. By combining these two parameters we should be able to increase the range of easily accessible nanoparticles using this approach. The smallest particles we formed, at 19 nm, are approaching the 10 nm cut-off for the loss of paramagnetism, which we wish to avoid. However, these particles have very promising subtle magnetic characteristics that could make them very useful for applications in imaging and biomedicine. With these molecules in hand, we wished to further evaluate their biomedical compatibility.

3.3 Biological evaluation:

We previously demonstrated that the materials were relatively non-toxic to mammalian cells through a standard MTT assay, at even reasonably high concentrations (up to 200 µg/mL).[21] Herein, we wish to report further studies that have better characterized their biological behaviour. As noted in the XRD data, these magnetite nanoparticles appear to be contaminated with hydroperoxide moieties. This makes them promising potential oxidizing agents, and they could possibly act novel antibacterial tools to complement existing therapies. For the following studies we used the 19 nm nanoparticles created at pH=13 exclusively. As they had been thoroughly washed and dried prior to storage, the pH of all solutions described below were done either in buffer or distilled water (pH=7).

Ampicillin and chloramphenicol were used as positive controls; both are potent, but older, front-line drugs with broad-spectrum activity.[51] The study was carried out as described in the experimental section above. The mean inhibitory concentrations of the different therapies were determined using serial dilutions of a stock of sonicated nanoparticles to provide the data summarized in Table 3.

Table 3. Minimum inhibitory concentration of the 19 nm nanomagnetite and two positive controls. Error represents the standard error of the mean.

Bacterial Species	**Minimum inhibitory concentration of the antibacterial agent (µg/mL)**		
	Nanomagnetite (A)	Ampicillin	Chloramphenicol
E. coli	2.79±0.37	0.78±0.09	0.42±0.05
S. aureus	2.02±0.47	0.85±0.11	0.46±0.05

The nanomagnetite shows potent antibacterial activity with an MIC of about 2.5 µg/mL against both gram-positive and gram-negative bacteria indicating that it is a broad-spectrum antibiotic. This makes it only about three times weaker an antibiotic than ampicillin, or six times weaker than chloramphenicol. The obviously different mechanism of action, however, makes it a potential co-therapy for antibiotic resistant strains, and further studies are required to determine the scope and potential of this material. This level of potency certainly deserves further study to determine the rationale for this difference in activity compared to that often observed for coated magnetite nanoparticles. It is notable that this antibacterial MIC is about 100-fold lower than the minimum mammalian cytotoxic dose we calculated from our MTT assay, suggesting that a large therapeutic window exists for this material.

Promising as this data is, the toxicity of the materials in our mammalian MTT assay was still non-negligible. The exact mechanism of cellular damage is of significant interest. One possibility is that the hydroperoxide groups are interfering with the anti-oxidant protection systems in cells. An important enzyme in this pathway is catalase, the enzyme responsible for the rapid decomposition of hydroperoxide to water and oxygen. If catalase activity is inhibited, one of the readily detectable effects is an increase in lipid peroxidation, which leads to damage to the cell membrane and subsequent cell-death.[52]

To examine this possible mechanism of action, serum catalase activity and lipid peroxidation levels were measured using a Wistar rat model. Forty rats were divided into four groups (n=10). The control group was given an oral gavage of 1 mL of distilled water in two portions every day for 14 days. The second group received the same treatment, except the solution contained 10 ppm of the 19 nm nanoparticles (10 µg/mL). The third group received 100 ppm/day, and the fourth group 1000 ppm/day. After 14 days, the rats were sacrificed and serum samples were analysed. The wide range of concentrations was

chosen based on spanning the range from the antibiotic-active concentration through the concentrations observed to be toxic by the MTT assay.

At the 10 µg/mL dose, there is no effect on the catalase activity. However, as the concentration increases, catalase activity declines. Although statistically significant, the clinical relevance of these changes remains uncertain as at 100 µg/mL, lipid peroxidation is still statistically identical to the control population (Figure 6), although catalase activity has dropped by over 25 %. At the highest dose, catalase activity has fallen off by over 40 %, and the levels of lipid peroxidation have increased two-fold. The actual hepatic and serum concentration levels of the nanoparticles requires further study to determine the lifetime of the materials in the liver before clearance, and their precise dispersal in the body.

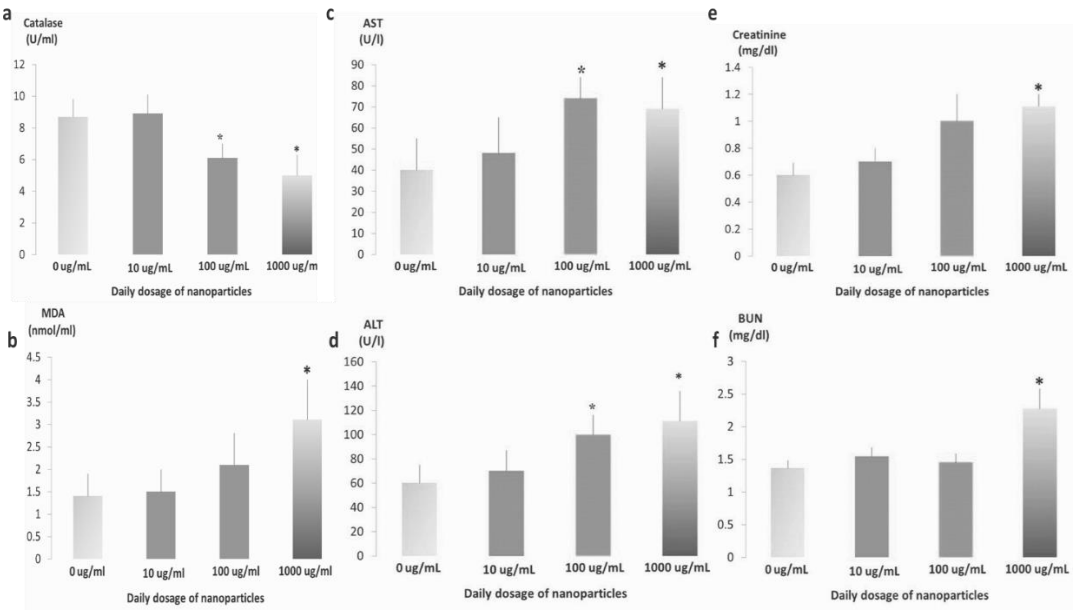

Figure 6. Results of the *in* vivo assays. In all cases the x-axis represents rats treated with different doses of nanoparticles; error represents the standard deviation (n=10); an asterisk (*) denotes a statistically significant difference ($p<0.05$) from the negative, untreated, control. **a)** Catalase activity in the rats treated with different daily doses of the nanoparticles; **b)** Lipid peroxidation levels, as estimated by end-product malondialdehyde (MDA) levels, in the rats treated with different daily doses of the nanoparticles; **c)** AST serum liver enzyme levels in rats treated with different daily doses of the nanoparticles; **d)** ALT serum liver

enzyme levels in rats treated with different daily doses of the nanoparticles; **e**) Serum creatinine levels in rats treated with different daily doses of the nanoparticles; **f)** Serum BUN levels in rats treated with different daily doses of the nanoparticles.

As an initial investigation of these effects we looked at several diagnostic enzymatic and biometric markers of both liver and kidney function. Alanine and aspartate aminotransferases (ALT and AST respectively) are produced in liver cells, and if these cells are damaged, can escape into the serum. Consequently, they are the well-established, "classic" tools to measure acute liver damage, although absolute values should not be used to indicate loss of function.[53] Similarly, serum creatinine[54] and total blood urea nitrogen (BUN),[55] are well established markers for similar damage to kidney cells. Although there are serious complications in using these markers in human clinical populations as a snapshot view of organ function due to genetic and diet variability, these remain excellent tools for investigating organ damage in animal models where genetic variability is limited and the diet and living conditions are rigorously controlled.

The liver studies are provided in Figure 10. As with the catalase activity measured above, the 10 μg/mL dosage does not have a statistically significant effect on the levels of either ALT or AST. However, although like for the catalase activity, we note a significant increase for the rats provided with a 100 μg/mL daily dose, the levels do not appear to worsen at 1000 μg/mL.

Renal health, as approximated by SRT and BUN levels (Figure 6), appears to be less sensitive to the nanoparticles than that of the liver. There is no clear statistically relevant increase in either creatinine or BUN levels until the highest dose of nanoparticles is administered. This is consistent with literature reports that suggest nanomagnetite clearance is mostly through the liver and spleen.[56]

A complicating fact not accounted for in this study is the expected protein agglomeration to the surface of unfunctionalized nanoparticles;[57, 58] this would be expected to limit their surface effects in biological systems. However, this effect did not appear to inhibit their bacterial inhibition activity. The fate of the particles in biological systems is currently under further investigation in our laboratories. The observation that toxicity was observed at the same concentration to mammalian cells in both the *in vitro* and *in vivo* assays suggests that the effect of protein agglomeration may prove minimal under the conditions of the study. However, further studies are required to better delineate the risk/benefit profile of these materials for biological applications to supplement these preliminary findings.

4. Conclusions:

Magnetite (Fe_3O_4) nanoparticles were prepared using a green, surfactant-free electrochemical methodology. Increased pH was found to slow the reaction leading to smaller nanoparticles (19 nm at pH=13 vs 23 nm at pH=10). These materials were characterized using XRD, FT-IR, and vibrational magnetometry. Computational calculations were also carried out to study the structural, magnetic and spectroscopic properties of our magnetite cluster models, containing up to 9 iron atoms. Models with a larger number of iron atoms are better able to predict to the vibrational frequencies that were observed experimentally. These systems might prove to be useful minimum clusters for further computational investigations into magnetite and form the basis of even larger clusters approximating the size of small nanoparticles, to better model experimental behaviour. The unusual hydroperoxide surface functionalization appears to provide a reactive material. The small size of these particles imparts unusual magnetic properties, as magnetic remanence and saturation decrease significantly with only a 4 nm difference

in diameter. This may be related to the level of crystallinity of the materials as a similar change in magnetic properties was not observed for a similar change in diameter in our previous study. These materials were then biologically evaluated and determined to be potent antibacterial agents with a MIC similar to the antibiotics ampicillin and chloramphenicol, and this concentration is approximately 100-fold more dilute than the MTT-determined cytotoxic concentration. The mechanism of cytotoxicity was hypothesized to be via oxidative damage, as the highly oxidized iron species are known to lead to lipid peroxidation an eventually cell death.[59, 60] Treatment of a rat model with differing concentrations of the nanoparticles demonstrated that 100 μg/mL/day was sufficient to statistically impact the levels of catalase in the serum, and a dose of 1000μg/mL/day was sufficient to increase the levels of lipid peroxidation. We also noted that hepatic damage accelerates around 100 μg/mL, while the kidney appears to be an order of magnitude less sensitive, possibly indicating the dominant route of clearance is through the liver. These toxic thresholds are similar to those observed in our previous MTT assay using mammalian cells. These off-target effects, and any bioaccumulation, will need to be better studied to determine the possibility of using these readily prepared nanoparticles for antibiotic or other biomedical applications.

Acknowledgments:

J.F.T and S.M.T would like to thank the University of Windsor for providing funding for this project. This work was made possible by the facilities of the Shared Hierarchical Academic Research Computing Network (SHARCNET: www.sharcnet.ca) and Compute/Calcul Canada. M.A. and F.S. would like to thank the University of Sistan and Baluchestan for financial support for this work. A.R., M.R.H. and M.J. would like to thank the University of Zabol for financial support for this work. All authors would like

to thank Katelyn Lei, University of Windsor, for the design and preparation of the Table of Contents graphic. All authors declare that they have no competing financial interest.

Supporting Information:

Supplementary material (Experimental details, coordinate and thermochemical data for all the optimized cluster models, raw biological data for antibacterial analyses, liver-related enzyme activity, catalase and oxidative damage, and markers of kidney damage (PDF)) is available in the online as a Data In Brief article accompanying this publication at: XXXXXX.

[1] K.A. Kydralieva, G.I. Dzhardimalieva, A.A. Yurishcheva, S.J. Jorobekova, Nanoparticles of magnetite in polymer matrices: Synthesis and properties, J. Inorg. Organomet. Polym. Mater., 26 (2016) 1212-1230.
[2] C. Su, Environmental implications and applications of engineered nanoscale magnetite and its hybrid nanocomposites: A review of recent literature, J. Hazard. Mater., 322 (2016) 48-84.
[3] A. Ali, M. Ahmad, M.N. Akhtar, S.F. Shaukat, G. Mustafa, M. Atif, W.A. Farooq, Magnetic nanoparticles (Fe3O4 & Co3O4) and their applications in urea biosensing, Russ. J. Appl. Chem., 89 (2016) 517-534.
[4] J. Shan, L. Wang, H. Yu, J. Ji, W.A. Amer, Y. Chen, G. Jing, H. Khalid, M. Akram, N.M. Abbasi, Recent progress in Fe_3O_4 based magnetic nanoparticles: From synthesis to application, Mater. Sci. Technol., 32 (2016) 602-614.
[5] V.L. Nguyen, Y. Yang, T. Teranishi, C.M. Thi, Y. Cao, M. Nogami, Biomedical applications of advanced multifunctional magnetic nanoparticles, J. Nanosci. Nanotechnol., 15 (2015) 10091-10107.
[6] I. Hussain, N.B. Singh, A. Singh, H. Singh, S.C. Singh, Green synthesis of nanoparticles and its potential application, Biotechnol. Lett., 38 (2016) 545-560.
[7] J.-K. Xu, F.-F. Zhang, J.-J. Sun, J. Sheng, F. Wang, M. Sun, Bio and nanomaterials based on Fe_3O_4, Molecules, 19 (2014) 21506-21528.
[8] J. Li, X. Shi, M. Shen, Hydrothermal synthesis and functionalization of iron oxide nanoparticles for MR imaging applications, Part. Part. Syst. Charact., 31 (2014) 1223-1237.
[9] M.B. Gawande, P.S. Branco, R.S. Varma, Nano-magnetite (Fe_3O_4) as a support for recyclable catalysts in the development of sustainable methodologies, Chem. Soc. Rev., 42 (2013) 3371-3393.
[10] S.C.N. Tang, I.M.C. Lo, Magnetic nanoparticles: Essential factors for sustainable environmental applications, Water Res., 47 (2013) 2613-2632.
[11] N.J. Tang, W. Zhong, H.Y. Jiang, X.L. Wu, W. Liu, Y.W. Du, Nanostructured magnetite (Fe_3O_4) thin films prepared by sol–gel method, J. Magn. Magn. Mater., 282 (2004) 92-95.
[12] S. Ni, X. Wang, G. Zhou, F. Yang, J. Wang, Q. Wang, D. He, Hydrothermal synthesis of Fe_3O_4 nanoparticles and its application in lithium ion battery, Mater. Lett., 63 (2009) 2701-2703.
[13] H. Karami, Synthesis and characterization of iron oxide nanoparticles by solid state chemical reaction method, J. Cluster Sci., 21 (2010) 11-20.
[14] D. Chen, S. Ni, Z. Chen, Synthesis of Fe_3O_4 nanoparticles by wet milling iron powder in a planetary ball mill, China Particuol., 5 (2007) 357-358.
[15] W.S. Chiu, S. Radiman, M.H. Abdullah, P.S. Khiew, N.M. Huang, R. Abd-Shukor, One pot synthesis of monodisperse Fe_3O_4 nanocrystals by pyrolysis reaction of organometallic compound, Mater. Chem. Phys., 106 (2007) 231-235.
[16] A.B. Chin, I.I. Yaacob, Synthesis and characterization of magnetic iron oxide nanoparticles via w/o microemulsion and Massart's procedure, J. Mater. Process. Technol., 191 (2007) 235-237.
[17] L. Cabrera, S. Gutierrez, N. Menendez, M.P. Morales, P. Herrasti, Magnetite nanoparticles: Electrochemical synthesis and characterization, Electrochim. Acta, 53 (2008) 3436-3441.

[18] S. Franger, P. Berthet, O. Dragos, R. Baddour-Hadjean, P. Bonville, J. Berthon, Large influence of the synthesis conditions on the physico-chemical properties of nanostructured Fe_3O_4, J. Nanopart. Res., 9 (2007) 389-402.
[19] A. Ahniyaz, G.A. Seisenbaeva, L. Häggström, S. Kamali, V.G. Kessler, P. Nordblad, C. Johansson, L. Bergström, Preparation of iron oxide nanocrystals by surfactant-free or oleic acid-assisted thermal decomposition of a Fe(III) alkoxide, J. Magn. Magn. Mater., 320 (2008) 781-787.
[20] F. Fajaroh, H. Setyawan, W. Widiyastuti, S. Winardi, Synthesis of magnetite nanoparticles by surfactant-free electrochemical method in an aqueous system, Adv. Powder Technol., 23 (2012) 328-333.
[21] S.M. Taimoory, A. Rahdar, M. Aliahmad, F. Sadeghfar, M. Hashemzaei, J.F. Trant, Importance of the inter-electrode distance for the electrochemical synthesis of magnetite nanoparticles: Synthesis, characterization, and cytotoxicity, e-J. Surf. Sci. Nanotechnol., 15 (2017) 31-39.
[22] L. Zhou, J. Yuan, Y. Wei, Core-shell structural iron oxide hybrid nanoparticles: from controlled synthesis to biomedical applications, J. Mater. Chem., 21 (2011) 2823-2840.
[23] E.A. Kwizera, E. Chaffin, Y. Wang, X. Huang, Synthesis and properties of magnetic-optical core-shell nanoparticles, RSC Advances, 7 (2017) 17137-17153.
[24] E.D. Brown, G.D. Wright, Antibacterial drug discovery in the resistance era, Nature, 529 (2016) 336-343.
[25] T.U. Berendonk, C.M. Manaia, C. Merlin, D. Fatta-Kassinos, E. Cytryn, F. Walsh, H. Bürgmann, H. Sørum, M. Norström, M.-N. Pons, N. Kreuzinger, P. Huovinen, S. Stefani, T. Schwartz, V. Kisand, F. Baquero, J.L. Martinez, Tackling antibiotic resistance: The environmental framework, Nat. Rev. Microbiol., 13 (2015) 310-317.
[26] E.N. Taylor, K.M. Kummer, N.G. Durmus, K. Leuba, K.M. Tarquinio, T.J. Webster, Superparamagnetic Iron Oxide Nanoparticles (SPION) for the Treatment of Antibiotic-Resistant Biofilms, Small, 8 (2012) 3016-3027.
[27] P. Basnet, G.K. Larsen, R.P. Jadeja, Y.-C. Hung, Y. Zhao, α-Fe_2O_3 nanocolumns and nanorods fabricated by electron beam evaporation for visible light photocatalytic and antimicrobial applications, ACS Appl. Mater. Interfaces, 5 (2013) 2085-2095.
[28] M. Arakha, S. Pal, D. Samantarrai, T.K. Panigrahi, B.C. Mallick, K. Pramanik, B. Mallick, S. Jha, Antimicrobial activity of iron oxide nanoparticle upon modulation of nanoparticle-bacteria interface, Sci. Rep., 5 (2015).
[29] N. Tran, A. Mir, D. Mallik, A. Sinha, S. Nayar, T.J. Webster, Bactericidal effect of iron oxide nanoparticles on *Staphylococcus aureus*, Int. J. Nanomed., 5 (2010) 277-283.
[30] Y. Chen, N. Gao, J. Jiang, Surface matters: Enhanced bactericidal property of core–shell Ag–Fe_2O_3 nanostructures to their heteromer counterparts from one-pot synthesis, Small, 9 (2013) 3242-3246.
[31] K.J.M. Bishop, C.E. Wilmer, S. Soh, B.A. Grzybowski, Nanoscale Forces and Their Uses in Self-Assembly, Small, 5 (2009) 1600-1630.
[32] D.M. Sievert, P. Ricks, J.R. Edwards, A. Schneider, J. Patel, A. Srinivasan, A. Kallen, B. Limbago, S. Fridkin, Antimicrobial-resistant pathogens associated with healthcare-associated infections summary of data reported to the National Healthcare Safety Network at the Centers for Disease Control and Prevention, 2009–2010, Infect. Control Hosp. Epidemiol., 34 (2013) 1-14.
[33] M.J. Frisch, G.W. Trucks, H.B. Schlegel, G.E. Scuseria, M.A. Robb, J.R. Cheeseman, G. Scalmani, V. Barone, B. Mennucci, G.A. Petersson, H. Nakatsuji, M. Caricato, X. Li, H.P. Hratchian, A.F. Izmaylov, J. Bloino, G. Zheng, J.L. Sonnenberg, M. Hada, M. Ehara, K. Toyota, R. Fukuda, J. Hasegawa, M. Ishida, T. Nakajima, Y.

Honda, O. Kitao, H. Nakai, T. Vreven, J.A. Montgomery Jr., J.E. Peralta, F. Ogliaro, M.J. Bearpark, J. Heyd, E.N. Brothers, K.N. Kudin, V.N. Staroverov, R. Kobayashi, J. Normand, K. Raghavachari, A.P. Rendell, J.C. Burant, S.S. Iyengar, J. Tomasi, M. Cossi, N. Rega, N.J. Millam, M. Klene, J.E. Knox, J.B. Cross, V. Bakken, C. Adamo, J. Jaramillo, R. Gomperts, R.E. Stratmann, O. Yazyev, A.J. Austin, R. Cammi, C. Pomelli, J.W. Ochterski, R.L. Martin, K. Morokuma, V.G. Zakrzewski, G.A. Voth, P. Salvador, J.J. Dannenberg, S. Dapprich, A.D. Daniels, Ö. Farkas, J.B. Foresman, J.V. Ortiz, J. Cioslowski, D.J. Fox, Gaussian 09, Gaussian, Inc., Wallingford, CT, USA, 2009.
[34] Performance Standards for Antimicrobial Susceptibility Testing; Seventeenth Informational Supplement., Clinical and Laboratory Standards Institute, Wayne, PA, 2007.
[35] P.R. Murray, K.S. Rosenthal, M.A. Pfaller, Medical Microbiology, Mosby/Elsevier, Philadelphia, 2009.
[36] J. Noh, O.I. Osman, S.G. Aziz, P. Winget, J.-L. Brédas, Magnetite Fe_3O_4 (111) surfaces: impact of defects on structure, stability, and electronic properties, Chem. Mater., 27 (2015) 5856-5867.
[37] J.R. Hart, A.K. Rappe, S.M. Gorun, T.H. Upton, Ab initio calculation of the magnetic exchange interactions in (μ-oxo)diiron(III) systems using a broken symmetry wave function, Inorg. Chem., 31 (1992) 5254-5259.
[38] A. Caneschi, F. Fabrizi de Biani, L. Kloo, P. Zanello, Magnetic and redox properties in hydroxo- and alkoxo-bridged Fe(III) binuclear complexes: A density functional study, Int. J. Quantum Chem., 72 (1999) 61-71.
[39] Z. Chen, Z. Xu, L. Zhang, F. Yan, Z. Lin, Magnetic exchange interactions in oxo-bridged diiron(III) systems: Density functional calculations coupling the broken symmetry approach, J. Phys. Chem. A, 105 (2001) 9710-9716.
[40] A.I. Ermakov, I.V. Yurova, A.D. Davydov, B.A. Khorishko, A.P. Lar'kov, K.V. Stanislavchik, The structure of minimal magnetite cluster, Russ. J. Gen. Chem., 83 (2013) 1493-1500.
[41] Y. Tian, B. Yu, X. Li, K. Li, Facile solvothermal synthesis of monodisperse Fe_3O_4 nanocrystals with precise size control of one nanometre as potential MRI contrast agents, J. Mater. Chem., 21 (2011) 2476-2481.
[42] N. Nishida, S. Amagasa, Y. Kobayashi, Y. Yamada, Synthesis of superparamagnetic δ-FeOOH nanoparticles by a chemical method, Appl. Surf. Sci., 387 (2016) 996-1001.
[43] A. Rahdar, M. Aliahmad, Y. Azizi, NiO nanoparticles: Synthesis and characterization, J. Nanostruct., 5 (2015) 145-151.
[44] O.A. Attallah, M.A. Al-Ghobashy, M. Nebsen, M.Y. Salem, Removal of cationic and anionic dyes from aqueous solution with magnetite/pectin and magnetite/silica/pectin hybrid nanocomposites: kinetic, isotherm and mechanism analysis, RSC Adv., 6 (2016) 11461-11480.
[45] F. Ju, Y. Hu, Removal of EDTA-chelated copper from aqueous solution by interior microelectrolysis, Sep. Purif. Technol., 78 (2011) 33-41.
[46] C. Morterra, A. Chiorlno, E. Borello, An IR spectroscopic characterization of α-FeOOH (goethite), Mater. Chem. Phys., 10 (1984) 119-138.
[47] M. Abareshi, E.K. Goharshadi, S. Mojtaba Zebarjad, H. Khandan Fadafan, A. Youssefi, Fabrication, characterization and measurement of thermal conductivity of Fe_3O_4 nanofluids, J. Magn. Magn. Mater., 322 (2010) 3895-3901.
[48] R.M. Cornell, U. Schwertmann, Electronic, Electrical and Magnetic Properties and Colour, The Iron Oxides, Wiley-VCH Verlag GmbH & Co. KGaA2004, pp. 111-137.

[49] Q.A. Pankhurst, J. Connolly, S.K. Jones, J. Dobson, Applications of magnetic nanoparticles in biomedicine, J. Phys. D: Appl. Phys., 36 (2003) R167.
[50] J. Orna, L. Morellon, P. Algarabel, J.M. De Teresa, A. Fernandez-Pacheco, G. Simon, C. Magen, J.A. Pardo, M.R. Ibarra, Fe_3O_4 epitaxial thin films and heterostructures: Magnetotransport and magnetic properties, Adv. Sci. Technol., 67 (2010) 82-91.
[51] I. Brook, Treatment of anaerobic infection, Expert Rev. Anti-Infect. Ther., 5 (2007) 991+.
[52] K. Jomova, M. Valko, Advances in metal-induced oxidative stress and human disease, Toxicology, 283 (2011) 65-87.
[53] J.R. Senior, Alanine aminotransferase: A clinical and regulatory tool for detecting liver injury–past, present, and future, Clin. Pharmacol. Ther. (Hoboken, NJ, U. S.), 92 (2012) 332-339.
[54] R.D. Perrone, N.E. Madias, A.S. Levey, Serum creatinine as an index of renal function: new insights into old concepts, Clin. Chem., 38 (1992) 1933-1953.
[55] V.S. Vaidya, M.A. Ferguson, J.V. Bonventre, Biomarkers of acute kidney injury, Annu. Rev. Pharmacol. Toxicol., 48 (2008) 463-493.
[56] T.K. Jain, M.K. Reddy, M.A. Morales, D.L. Leslie-Pelecky, V. Labhasetwar, Biodistribution, clearance, and biocompatibility of iron oxide magnetic nanoparticles in rats, Mol. Pharmaceutics, 5 (2008) 316-327.
[57] T. Cedervall, I. Lynch, S. Lindman, T. Berggård, E. Thulin, H. Nilsson, K.A. Dawson, S. Linse, Understanding the nanoparticle–protein corona using methods to quantify exchange rates and affinities of proteins for nanoparticles, Proc. Natl. Acad. Sci. U. S. A., 104 (2007) 2050-2055.
[58] S. Tenzer, D. Docter, J. Kuharev, A. Musyanovych, V. Fetz, R. Hecht, F. Schlenk, D. Fischer, K. Kiouptsi, C. Reinhardt, K. Landfester, H. Schild, M. Maskos, S.K. Knauer, R.H. Stauber, Rapid formation of plasma protein corona critically affects nanoparticle pathophysiology, Nat. Nano., 8 (2013) 772-781.
[59] C.G. Fraga, B.E. Leibovitz, A.L. Tappel, Lipid peroxidation measured as thiobarbituric acid-reactive substances in tissue slices: characterization and comparison with homogenates and microsomes, Free Radical Biology and Medicine, 4 (1988) 155-161.
[60] U.S. Gaharwar, R. Meena, P. Rajamani, Iron oxide nanoparticles induced cytotoxicity, oxidative stress and DNA damage in lymphocytes, Journal of Applied Toxicology, 37 (2017) 1232-1244.